Subunit Exchange by CheA Histidine Kinases from the Mesophile *Escherichia coli* and the Thermophile *Thermotoga maritima*†

Sang-Youn Park,‡ Cindy M. Quezada,§ Alexandrine M. Bilwes,‡ and Brian R. Crane*,‡

Department of Chemistry and Chemical Biology, Cornell University, Ithaca, New York 14853, and Division of Biology, The California Institute of Technology, Pasadena, California 91125

Received July 15, 2003; Revised Manuscript Received December 16, 2003

ABSTRACT: Dimerization of the chemotaxis histidine kinase CheA is required for intersubunit autophosphorylation [Swanson, R. V., Bourret, R. B., and Simon, M. I. (1993) *Mol. Microbiol. 8*, 435−441]. Here we show that CheA dimers exchange subunits by the rate-limiting dissociation of a central four-helix bundle association domain (P3), despite the high stability of P3 versus unfolding. P3 alone determines the stability and exchange properties of the CheA dimer. For CheA proteins from the mesophile *Escherichia coli* and the thermophile *Thermotoga maritima*, subunit dissociation activates at temperatures where the respective organisms live (37 and 80 °C). Under destabilizing conditions, P3 dimer dissociation is cooperative with unfolding. Chemical denaturation is reversible for both EP3 and TP3. Aggregation accompanies thermal unfolding for both proteins under most conditions, but thermal unfolding is reversible and two-state for EP3 at low protein concentrations. Residue differences within interhelical loops may account for the contrasted thermodynamic properties of structurally similar EP3 and TP3 (41% sequence identity). Under stabilizing conditions, greater correlation between activation energy for dimer dissociation and P3 stability suggests more unfolding in the dissociation of EP3 than TP3. Furthermore, destabilization of extended conformations by glycerol slows relative dissociation rates more for EP3 than for TP3. Nevertheless, at physiological temperatures, neither protein likely unfolds completely during subunit exchange. EP3 and TP3 will not exchange subunits with each other. The receptor coupling protein CheW reduces the subunit dissociation rate of the *T. maritima* CheA dimer by interacting with the regulatory domain P5.

In the signal transduction pathway of bacterial chemotaxis, the binding of attractants and repellants to transmembrane receptors regulates the histidine kinase CheA (*1*−*4*). Dimeric CheA initiates a cytoplasmic phosphorelay by transferring phosphate from ATP bound within its kinase domain (P4) to a specific histidine residue on a separate domain (P1) of the adjacent subunit. The phosphate then transfers to an aspartyl residue on the response regulator CheY, which diffuses from the membrane to modulate the flagellar motor. Five domains (P1−P5) comprise CheA (*5*−*7*). P1 contains the substrate histidine, P2 docks CheY for phosphotransfer from P1 to CheY, P3 mediates dimerization, P4 binds ATP, and P5 regulates kinase activity in response to chemoreceptors through binding of the receptor-coupling protein CheW (*8*). Because signal transduction depends on CheA transphosphorylation (*5*, *9*), the physical properties of the CheA dimerization domain and the functional consequences of subunit exchange merits investigation.

The crystal structure of *T. maritima* CheA Δ289[1] (domains P3 to P5) defined P3 as a four-helix bundle formed by the parallel association of two helical hairpins, one supplied by each subunit (Figure 1A,B) (*6*). Two small N-terminal β-strands cross and cap the P3 barrel. The parallel arrangement of helices in a dimeric four-helix bundle is uncommon, but found also in the cytoplasmic domain of the chemoreceptors (Figure 1C) (*10*, *11*). In P3, an extensive hydrophobic interface (∼2000 Å^2 per subunit) generates a large energy barrier for dissociation of the subunits (*6*). Furthermore, subunit dissociation should destabilize the native P3 structure by disrupting the hydrophobic core at the dimer interface.

Nevertheless, CheA subunits exchange with one another (*12*) and CheA loses activity on dilution in a manner consistent with dissociation to an inactive CheA monomer (*13*). Thus, CheA subunit exchange raises interesting questions: Is CheA dimer dissociation responsible for subunit exchange? Does this process concur with complete unfolding of the P3 domain under physiological conditions? Or, in contrast, does subunit exchange involve association of dimers and swapping of subunits to avoid unfavorable structural transitions? If P3 does unfold on subunit dissociation, is specificity maintained during reassociation?

† This work was supported by a National Institute of Health Grant (GM066775) to B.R.C.

* To whom correspondence should be addressed. E-mail: bc69@cornell.edu.

‡ Cornell University.

§ The California Institute of Technology.

[1] Abbreviations: TP3, *Thermotoga maritima* P3 domain; EP3, *Escherichia coli* P3 domain; Δ289, *T. maritima* P3−P4−P5 domain; Δ258, *E. coli* P3−P4−P5 domain; Tsr, chemotaxis serine receptor; GF, gel filtration; T_m, melting temperature; ITC, isothermal titration calorimetry; ASA, accessible surface area; C_p, heat capacity; CD, circular dichroism; DSC, differential scanning calorimetry; η, viscosity coefficient; U, unfolded state; N, native folded state; TS_d, transition state for subunit dissociation; TS_U, transition state for unfolding; K_D, dissociation equilibrium constant; GdnHCl, guanidine hydrogen chloride; ΔG change in Gibb's free energy; ΔH, change in enthalpy; ΔS, change in entropy.

10.1021/bi0352419 CCC: $27.50
Published on Web 02/07/2004

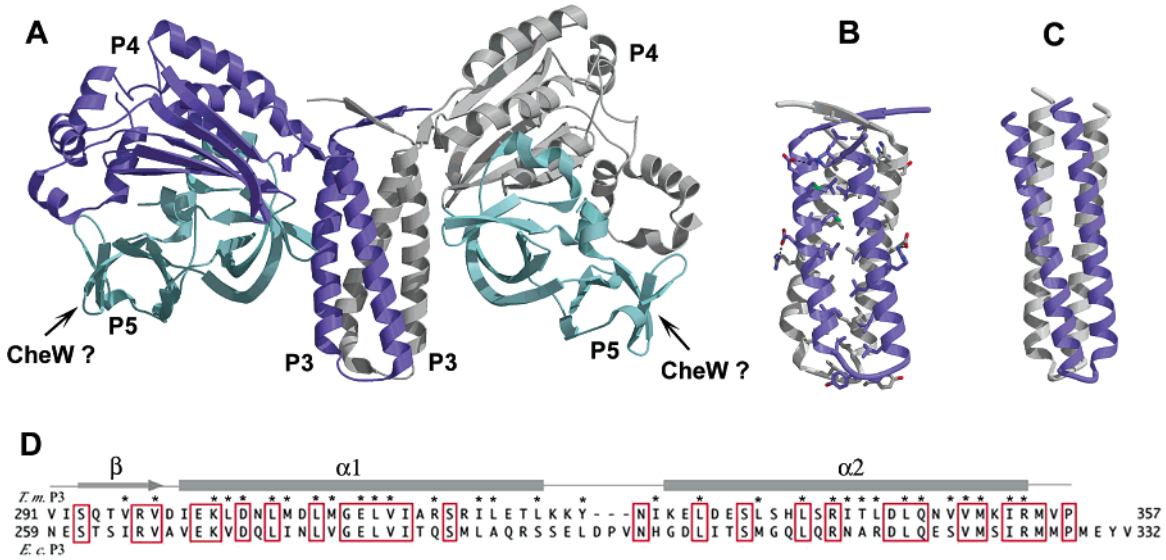

FIGURE 1: Ribbon diagrams for structures of *T. maritima* CheA Δ289 (A), P3 (B), and *E. coli* Tsr receptor cytoplasmic fragment (C). (A) Dimeric CheA Δ289 (blue and gray subunits, PDB code 1B3Q) has three domains (P3, P4, and P5): P3 mediates dimerization, P4 binds ATP, and P5 interacts with CheW. A putative CheW binding site is shown at the end of P5. (B) The P3 domain is composed of two symmetrical helix hairpins that associate via an exclusively hydrophobic interface (side chains shown). (C) Cytoplasmic domain of the Tsr chemoreceptor (PDB code 1QU7) has a similar structure to P3. Only the end of the ∼260 Å cytoplasmic receptor fragment is shown. (D) *T. maritima* P3 and *E. coli* P3 have high sequence similarity (identities in red), especially for residues that participate in the dimer interface (∗).

Protein conformational changes range greatly in form and amplitude. The most drastic examples involve either local or global folding transitions of the polypeptide (*14*). The role of induced folding in oligomerization, molecular recognition, and protein aggregation impacts cellular events ranging from signal transduction cascades to amyloid-based disease (*14*, *15*). Dimeric coiled coils that form two- or four-helix bundles can mediate transient protein interactions important for function. For example, heterodimerization of two-helix coiled coils regulates leucine zipper transcription factors (*16*), and heterooligomerization of four-helix coiled coils regulates vesicle fusion (*17*). To investigate the general mechanism of how stable four-helix dimers exchange subunits and the physical implications of undergoing such transitions, we have carried out kinetic and thermodynamic studies of subunit exchange by CheA proteins from two organisms that grow at vastly different temperatures: *Escherichia coli* (optimal growth temperature: 37 °C) and *Thermotoga maritima* (optimal growth temperature: 80 °C (*18*)). We also evaluate how these exchange reactions are affected by the receptor-coupling protein CheW.

MATERIALS AND METHODS

Cloning, Expression, and Purification. PCR-amplified fragments of DNA encoding *Thermotoga maritima* CheA Δ289 (290−671), *T. maritima* CheW, and *E. coli* CheA Δ258 (259−654) were subcloned into the pET28a vector (Novagen), expressed in *E. coli* BL21(DE3) and purified by Ni^{2+} chelate chromatography followed by gel filtration as previously described (*7*). Constructs for *T. maritima* CheA P3 (290−357) and *E. coli* CheA P3 (259−332) were obtained by the introduction of a stop codon by Quickchange mutagenesis (Stratagene) at position 358 and 333 in the background of pET28a constructs expressing *T. maritima* CheA Δ289 and *E. coli* CheA Δ258, respectively. Purified proteins were stored in Gel Filtration (GF) buffer (50mM Tris pH 7.5, 150 mM NaCl). *T. maritima* CheA Δ289 and *T. maritima* CheW coeluted as a complex on GF (Superdex200). Concentrations of proteins were measured spectrophotometrically on the basis of the following extinction coefficients (ϵ) at 280 nm. For *T. maritima*: CheA Δ289 (21620 $M^{-1}cm^{-1}$), CheA P3 (2560 $M^{-1}cm^{-1}$) CheW (1280 $M^{-1}cm^{-1}$). For *E. coli*: CheA Δ258 (24180 $M^{-1}cm^{-1}$), CheA P3 (2560 $M^{-1}cm^{-1}$). Extinction coefficients were calculated from the number of tryptophan and tyrosine residues present in each protein (*19*).

Kinetics of Subunit Exchange Analyzed by Gel Filtration Chromatography. To study the rates of CheA subunit exchange, we measured the conversion of homodimers of the P3 domain and Δ289 (P3−P4−P5) to heterodimers. The two reactants ($P3_2$ and $\Delta289_2$) and product (P3:Δ289) can be resolved by size on a GF column and then quantitated by measuring the area of their respective elution profiles (as monitored by absorbance at 280 nm). At low temperature (∼4 °C), the exchange reaction was slow enough to be negligible for both *T. maritima* P3 (TP3) and *E. coli* P3 (EP3), allowing the reactions to be quenched by flash-cooling in liquid nitrogen prior to characterization by GF at 4 °C. *T. maritima* CheA Δ289 and TP3 (or *E. coli* CheA Δ258 and EP3) were each diluted to 0.1, 0.2, or 0.3 mM with GF buffer in 110 μL and incubated for a given time at preset temperatures before the reactions were freeze quenched. Samples were subsequently thawed on ice and their content of product (P3:Δ289) and remaining reactants ($P3_2$ and $\Delta289_2$) analyzed by GF at 4 °C with an analytical column and an AKTA FPLC system (Pharmacia). Superose12 10/30 (Pharmacia) resolved the three protein species of *T. maritima*, but two Superdex75 10/30 (Pharmacia) connected in series were necessary to resolve the three different *E. coli* complexes. Similar experiments following incubation at different temperatures (*T. maritima*: 55−70 °C, *E. coli*: 22−

31 °C) characterized the temperature dependence of subunit exchange. Aggregation and precipitation of reactants prevented incubation at higher temperatures. Addition of glycerol directly to the GF buffer in varying concentrations probed the effect of a stabilizing agent on the exchange rates.

Data Analysis for Exchange Kinetics. From the gel filtration profiles, the concentrations of each protein complex were determined by fitting the three elution profiles representing $P3_2$, $\Delta289_2$, and P3:Δ289 to Gaussian curves followed by integration of their respective absorbance areas (KaleidaGraph). The integrated values were used with ϵ_{280} for each species (ϵ_{280} for P3:Δ289 was averaged from the ϵ_{280} values of $P3_2$ and $\Delta289_2$) to determine total moles in each peak. These values were converted to concentrations with knowledge of the initial reaction volume. For a dissociative mechanism, where dissociation is rate limiting, the observed rate constant for exchange (k_{obs}) equates with the rate constant for dimer dissociation (k_{-r}), if the two reactant concentrations are equal (Appendix 1).

$$[AB]_t = 2[A]_0[1 - e^{-k_{-r}t}] \quad (1)$$

where $[AB]_t$ = heterodimer concentration at time t and $[A]_0$ = the initial concentration of one homodimer, which is equal to the initial concentration of the other homodimer. We determined k_{-r} (Figure 3A, left) by fitting the time dependence of the integrated gel filtration profiles to eq 1 by nonlinear least squares (KaleidaGraph). Temperature dependence of k_{-r} was related to activation enthalpy and entropy for dissociation ($\Delta H^{\ddagger}_d$ and $\Delta S^{\ddagger}_d$, respectively) by an Eyring plot of eq 2.

$$k_{-r} = A \exp^{-\Delta G^{\ddagger}_d/RT} = A \exp^{-\Delta H^{\ddagger}_d/RT} \exp^{\Delta S^{\ddagger}_d/R} \quad (2)$$

Temperature dependencies of $\Delta H^{\ddagger}_d$ and $\Delta S^{\ddagger}_d$ were modeled with a temperature independent change in heat capacity ($\Delta C_p^{\ddagger}{}_d$, eqs 3 and 4) with T_{ref} taken as the lowest temperature in the experimental range.

$$\Delta H^{\ddagger}_d(T) = \Delta H^{\ddagger}_d(T_{ref}) + \Delta C_p^{\ddagger}{}_d(T - T_{ref}) \quad (3)$$

$$\Delta S^{\ddagger}_d(T) = \Delta S^{\ddagger}_d(T_{ref}) + \Delta C_p^{\ddagger}{}_d \ln(T/T_{ref}) \quad (4)$$

As the Eyring plots were close to linear for both TP3 and EP3, eq 2 substituted by eqs 3 and 4 provided too many parameters for a robust fitting by nonlinear least squares, so rather, $\Delta H^{\ddagger}_d$ and $\Delta S^{\ddagger}_d$ were determined by the linear approximation of eq 2. In the case of TP3, an estimate of $\Delta C_p^{\ddagger}{}_d$ was made from manually generating curves within the bounds of the experimental data. The prefactor in eq 2 (A) that reflects the barrier crossing frequency and affects the calculated $\Delta S^{\ddagger}_d$ and $\Delta G^{\ddagger}_d$ values was set to both the frequency of a bond vibration as given by canonical transition state theory ($A = k_B T/h = 6.2 \times 10^{12}$ s^{-1} at 25 °C (*20*)) and a slower frequency associated with chain diffusion and solvent friction in protein conformational change. Various estimates for this frequency have been suggested on experimental and theoretical grounds (*21*). We chose a value of 5×10^8 s^{-1} for the unimolecular unfolding reaction, which is in the range of intrachain diffusion for small peptides (*22*).

Thermodynamics of P3 Unfolding with Circular Dichroism (CD) Spectroscopy. To evaluate helical content, the change in P3 ellipticity at wavelength 222 nm with temperature or denaturant was measured with an AVIV Circular Dichroism Spectrometer (Model 62ADS) (cell pathlength = 1 mm, bandwidth = 1.5 nm, signal averaging time = 3−5 s, temperature step = 1 °C).

Thermal Denaturation. If subunit dissociation is cooperative with unfolding, the temperature at which half of the helical content is lost (T_m) should be concentration dependent. Thus, TP3 and EP3 thermal unfolding experiments were carried out with varying concentrations (5−20 μM) of protein in GF buffer. To test the effect of glycerol on stability, glycerol was also added to GF buffer in the same concentrations that were used for assaying the rates of subunit exchange.

Chemical Denaturation. Chemical unfolding experiments were performed by adding increasing amounts of guanidine HCl (GdnHCl) (0−5 M) to P3 samples, while holding the P3 concentration constant. To determine enthalpies and entropies of unfolding, each set of GdnHCl melts was taken at three different temperatures for TP3 and six different temperatures for EP3. A given GdnHCl concentration was successively raised to each temperature point and the CD signal measured 5 min after it had stabilized (which typically took 1−2 min). Equilibration for one hour longer had no further effect on the signal. GdnHCl concentrations were determined by refractive index measurements.

Data Analysis for Thermal and Chemical Unfolding. (i) Thermal Unfolding. To evaluate the cooperativity of the P3 unfolding reaction, concentration dependence of the T_m was monitored and fitted to eq 5 (*23*).

$$1/T_m = R/\Delta H_U \ln C_0 + (\Delta S_U - R \ln 2)/\Delta H_U \quad (5)$$

where C_0 is the P3 dimer concentration. On establishing a two-state model for EP3 unfolding, subsequent CD data were analyzed by assuming that dimer unfolding couples to chain dissociation and that no intermediate states are appreciably populated at equilibrium (N↔2U, where N is the folded subunit, U is the unfolded subunit of the dimer, and $K_U = [U]^2/[N]$). With a total subunit concentration of $C_0 = U + 2N$, the equilibrium constant becomes

$$K_U = 2C_0 f_u^{\,2}/(1 - f_u) \quad (6)$$

where f_u is fraction of unfolded subunit. The ellipticity at 222 nm reports on f_u through the expression

$$f_u = (\theta - \theta_{N_2})/(\theta_U - \theta) \quad (7)$$

where θ_{N_2} and θ_U are the mean residue ellipticities corresponding to the folded dimer and unfolded monomer, respectively. T_m is defined in the CD experiments as the temperature where $f_u = 0.5$. If the data analysis is limited to the vicinity of T_m,

$$K(T) = C_0 \exp[\Delta H/R(1/T_m - 1/T)] \quad (8)$$

from which the van't Hoff ΔH can be extracted by plotting ln K versus $1/T$ (*23*).

(ii) Chemical Unfolding. For chemical unfolding studies, equilibrium constant K_U was determined at each GdnHCl concentration and converted to ΔG_U by $\Delta G_U = -RT \ln K_U$, K_U being defined by eq 6.

ΔG_U was extrapolated to 0 M GdnHCl (ΔG_{H_2O}) by assuming a linear dependence of ΔG_U on denaturant concentration (Linear Extrapolation Model, LEM).

$$\Delta G = \Delta G_{H_2O} - m[\text{GdnHCl}] \quad (9)$$

ΔH_U, ΔS_U, and ΔC_{pU} were determined by fitting the temperature dependence ΔG_U to eq 10 by nonlinear least squares.

$$\Delta G_U(T) = \Delta H_U(T_{ref}) - T\Delta S_U(T_{ref}) + \Delta C_{pU}(T - T_{ref} - T\ln(T/T_{ref})) \quad (10)$$

Glycerol Perturbation of Stability and Subunit Exchange. Glycerol was used to perturb both P3 stability and subunit exchange rates. $\Delta\Delta G_U$ values for different glycerol concentrations were estimated by monitoring changes in T_m and applying eq 11 with reference to a condition of 0% glycerol (T_{m0}, ΔH_0, k_{-r0}; see Appendix 2).

$$\Delta\Delta G_U = [T_{m0} - T_m][\Delta H_0/T_{m0}] \quad (11)$$

$\Delta\Delta G_U$ depends on an estimate of ΔH_0 at T_{m0}. ΔH_0 for TP3 was chosen as the value obtained from reversible chemical denaturation extrapolated to T_m by application of ΔC_{pU}. For both proteins, ΔH_U so determined is in good agreement with the values derived from van't Hoff analyses of the respective melting curves. Values of $\Delta\Delta G_U$ so obtained were compared $\Delta\Delta G^{\ddagger}$ for subunit exchange as given by

$$\Delta\Delta G^{\ddagger} = -RT\ln(k_{-r}/k_{-r0}) \quad (12)$$

Evaluating the Dissociation Rate Constant (k_{-r}) in the Presence of CheW. CheW perturbed the rates of heterodimer formation by binding to Δ289 (no interaction was observed between P3 and CheW by isothermal titration calorimetry (ITC)). Under these circumstances there is not an analytical solution to the reaction scheme of Appendix 1. Thus, we used numerical integration algorithms of Chemical Kinetics Simulator (ver 1.01) to predict reaction kinetics while varying k_{-r} of $\Delta 289_2$. It was assumed that (1) CheW only affected the k_{-r} for $\Delta 289_2$, (2) k_r is much larger than k_{-r}, and (3) kinetic constants for $P3_2$ and P3:Δ289 were unaltered by the presence of CheW.

Statistical Thermodynamic Calculations of ΔC_p for Coiled-Coil Domain Unfolding. For a set of two- and four-helix bundle coiled coils (including EP3 and TP3), ΔC_{pU} was calculated by first determining the change in accessible surface area (ΔASA) of individual atoms upon unfolding the native structures. Atomic ΔASA values were scaled to empirically determined atomic ΔC_p values for changes in hydration of atoms defined as hydrophobic aromatic (ΔC_p^{arm}), hydrophobic aliphatic (ΔC_p^{alp}), and hydrophilic (ΔC_p^{hyd}), and changes in interactions of atoms defined as hydrophobic van der Waals ($\Delta C_p^{arm,vdw}$), aliphatic van der Waals ($\Delta C_p^{alp,vdw}$), and hydrogen bonding (ΔC_p^{HB}) with the following equations (*24*):

$$\Delta C_p^{hyd}(T, °C) = -1.27 + (8.04 \times 10^{-3})(T - 25) - (31.1 \times 10^{-6})(T - 25)^2 \text{ J K}^{-1}\text{ mol}^{-1}\text{ Å}^{-2} \quad (13a)$$

$$\Delta C_p^{alp}(T, °C) = 2.14 - (4.48 \times 10^{-3})(T - 25) - (2.5 \times 10^{-6})(T - 25)^2 \quad (13b)$$

$$\Delta C_p^{arm}(T, °C) = 1.55 - (5.47 \times 10^{-3})(T - 25) - (8.6 \times 10^{-6})(T - 25)^2 \quad (13c)$$

$$\Delta C_p^{alp,vdw}(T, °C) = -0.09 - (0.81 \times 10^{-3})(T - 25) - (4.34 \times 10^{-6})(T - 25)^2 \quad (13d)$$

$$\Delta C_p^{arm,vdw}(T, °C) = -0.09 - (1.19 \times 10^{-3})(T - 25) - (5.5 \times 10^{-6})(T - 25)^2 \quad (13e)$$

$$\Delta C_p^{HB}(T, °C) = -0.02 - (6.03 \times 10^{-3})(T - 25) - (92.0 \times 10^{-6})(T - 25)^2 \quad (13f)$$

ASAs for the native conformation were determined by application of the Lee and Richard's algorithm (*25*) as implemented in ACCESS (Scott R. Presnell, University of California, San Francisco) to native coordinates (determined by X-ray crystallography, NMR, or homology modeling), whereas ASAs for unfolded states were taken from estimates of the maximum and minimum exposure in the denatured polypeptide (*26*, *27*). The limit of minimum unfolded exposure gave better agreement to experimental ΔC_{pU} values and produced the values shown in Table 2.

Homology Modeling of EP3. A homology model for EP3 was produced with SWISS-MODEL (*28*) by aligning EP3 with TP3 as shown in Figure 1D (sequence identity 41%). As the helical periodicity of hydrophobic residues in the dimer interface is well conserved between TP3 and EP3, we expect the EP3 model to provide a good estimate of the relative amounts of polar and nonpolar surface area exposed on unfolding in comparison to TP3. The larger interhelical loop in EP3 was modeled as a small β-hairpin turn by SWISS-MODEL.

RESULTS

E. coli and T. maritima CheA Dimers Exchange Subunits at Temperatures Commensurate with the Living Conditions of the Respective Organisms. We monitored CheA subunit exchange by measuring the formation of heterodimers from homodimers of the P3 domain and homodimers of domains P3−P4−P5 (Δ289). Following temperature quenching of the exchange reaction, homodimer reactants and heterodimer products were separated by size and quantitated (Figure 2). The subunit exchange rates for both TP3 (0.001 s^{-1}, 55 °C) and EP3 (0.002 s^{-1}, 22 °C) are relatively slow and increase with temperature. P3 subunit exchange can be detected within 1 h at 22 °C for EP3 and within 1 h at 55 °C for TP3. At long times, product ratios equilibrate to a statistical 1:2:1 ratio of $P3_2$:(P3:Δ289):$\Delta 289_2$, indicating that the P4 and P5 domains of Δ289 have minimal effects on the P3 dimerization equilibrium (Figure 2B, inset). Similar stabilities for the three dimeric species is consistent with the crystal structure

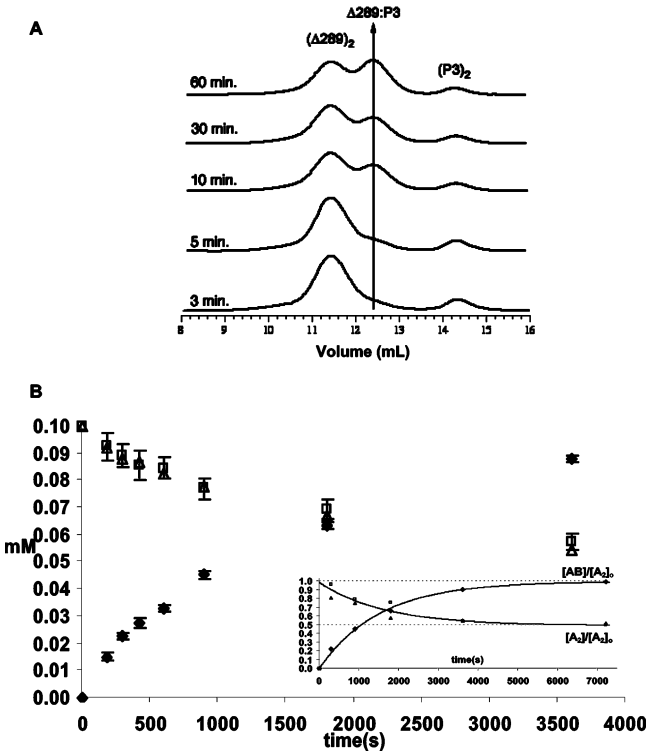

FIGURE 2: $\Delta289_2$ and $P3_2$ exchange subunits to generate heterodimer Δ289:P3. (A) Gel filtration chromatography (GF) of products after temperature-induced formation of *T. maritima* P3: Δ289 from $\Delta289_2$ and $P3_2$. $\Delta289_2$ and $P3_2$ were incubated for different time at 55 °C and then rapidly cooled by immersion in liquid nitrogen. Products were resolved at 4°C on Superose12. Initial concentrations of $\Delta289_2$ and $P3_2$ are equivalent; peak areas differ from different respective extinction coefficients. (B) Time course of the *T. maritima* CheA subunit exchange reaction. $\Delta289_2$(△) and $P3_2$(□) (0.1mM each) were mixed for increasing times at 55°C, flash cooled in liquid nitrogen, and then heterodimer products(◆) analyzed by GF. GF elution traces were fit to three Gaussian curves to quantitate products. At long times, $\Delta289_2$ (A_2) and $P3_2$ (B_2) concentrations ($[A_2] = [B_2]$) decreased to half of their initial starting concentrations and the heterodimer concentration([AB]) approached the initial concentration of the reactants indicating a statistical 1:2:1 ratio of products at equilibrium (inset).

of CheA Δ289, which shows that the P3 domains contribute 97% of the 3950 Å^2 of CheA dimer interface surface area.[2]

CheA Dimers Exchange Subunits by a Dissociative Process with a High Activation Barrier. Previous studies of the concentration dependence of CheA activity indicated that CheA dimers equilibrate with low concentrations of monomer (*13*). Nevertheless, stability of the P3 domain and the absence of detectable free subunits in solution motivated us to determine if association of dimers could facilitate subunit exchange of the highly stable *T. maritima* CheA. Subunit exchange could involve two general mechanisms: (1) dimers dissociate to monomers prior to reassociation; or (2) dimers associate with each other and swap subunits in a higher order complex (Figure 3A). These mechanisms predict substantially different rate dependencies on initial homodimer concentrations (Appendix 1). For a dissociative process, initial rates will scale with the concentration of one homodimeric species (provided the other has an equal concentration), whereas for a process involving association of two dimers, initial rates will scale with the product of the concentration of the two homodimers. Although both mechanisms predict a similar exponential decrease in heterodimer formation with time, only for the associative mechanism will the observed rate constant depend on the initial homodimer starting concentrations (Appendix 1). The subunit exchange rate in *T. maritima* CheA increases linearly with the concentration of each reactant (which are held equal to each other), and the observed rate constant is independent of initial reactant concentration (Figure 3C). The CheA reassociation rate constant (k_r) must be much greater than that for dissociation (k_{-r}) because the concentration of monomers in solution is very low. (We cannot detect free subunits by gel filtration, native gel electrophoresis, light-scattering or CD; and the dimer dissociation constant of *E. coli* CheA is small, (*13*)). Thus, CheA subunit exchange involves a mechanism where each homodimer dissociates slowly into monomers, which then rapidly reassociate into heterodimers (Figure 3A, left).

The kinetic model for subunit exchange by dissociation given in Appendix 1 does not assume that the rate constants for dissociation (k_{-r}) and association of the homodimers (k_r) equate with those of the heterodimer (k_{-h}, k_h). However, in our system, the ratios of rate constants (k_{-r}/k_r and k_{-h}/k_h) must be the same because at equilibrium the concentrations of reactants and products produces a statistical binomial distribution (Figure 2B). As these species all contain the same P3 association domain, whose intermolecular contacts almost solely compose the CheA dimer interface, it is likely that $k_{-r} = k_{-h}$ and $k_r = k_h$. Under these circumstances, the observed rate constant of heterodimer formation (k_{obs}) equates to k_{-r} (Appendix 1).

The concentration dependence of the exchange reaction was determined only with *T. maritima* CheA proteins because of their slower exchange kinetics relative to *E. coli* CheA and the difficulty in resolving the *E. coli* species at higher concentrations (see Methods). However, it is likely that the *E. coli* proteins also exchange by subunit dissociation as their dimers are less stable than those of *T. maritima* (see below). Furthermore, concentration dependence of activity and cross-linking studies have previously determined that *E. coli* CheA dimers dissociate under physiological conditions (*13*). Interestingly, despite conservation of most dimer interface residues by TP3 and EP3, the two proteins will not exchange subunits with each other.

The temperature dependence of the exchange reaction reflects the activation parameters for the rate-limiting step of dimer dissociation. The temperature dependence is Arrhenius and can be fitted to an expression of transition-state (TS) theory that relates k_{-r} to the free energy ($\Delta G^{\ddagger}_d$), enthalpy ($\Delta H^{\ddagger}_d$), and entropy ($\Delta S^{\ddagger}_d$) necessary to obtain the activated complex for dissociation (eq 2, Figure 4) (*20*). The values of $\Delta G^{\ddagger}_d$ and $\Delta S^{\ddagger}_d$ depend on assigning a barrier crossing frequency to the preexponential factor of eq 2. In canonical TS theory, this value reflects a bond vibration ($\sim 10^{13}$ s^{-1} (*20*)); however, for protein folding, lower frequencies associated with rates of chain diffusion and solvent friction ($10^6 - 10^8$ s^{-1}) are probably more appropriate (*21*). The values

[2] At equal concentrations (5 μM), CheA Δ289 and TP3 have similar T_m values (92 and 90 °C, respectively). The Δ289 melting curve also fits a two-state unfolding mechanism and is more reversible than that of TP3 alone. Although these data suggest that TP3 stability does not differ significantly in Δ289, overlapping unfolding transitions of the three Δ289 domains complicates deconvolution of TP3 thermodynamic properties in the context of the larger protein.

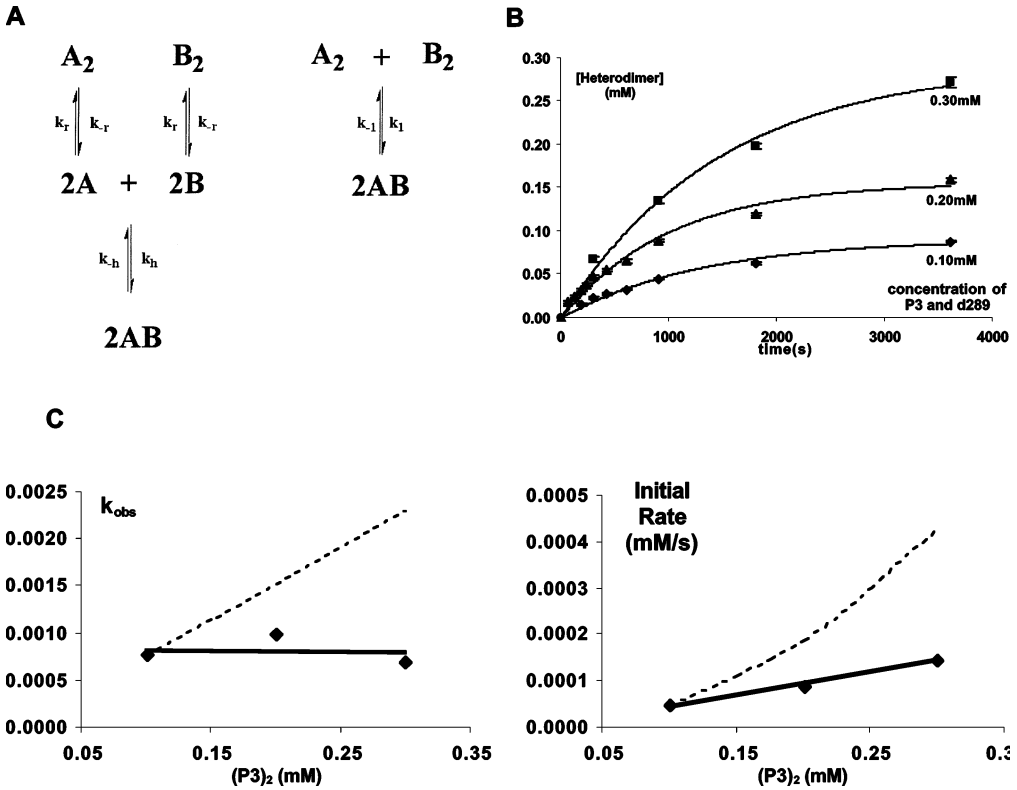

FIGURE 3: Possible mechanisms for CheA dimer exchange. (A) Dissociative (left) and associative (right) mechanisms for subunit exchange. Although A_2 and B_2 are distinct chemical species, they share the same dimerization domain, and thus, this scheme assumes that A_2 and B_2 have the same rate constants for dissociation (k_{-r}) and association (k_r). (B) Heterodimer formation at three different starting concentrations of *T. maritima* $P3_2$ and $\Delta289_2$ (◆, 0.1 mM; ▲, 0.2 mM; ■, 0.3 mM; 55°C). Data are fit to the exponential decay function of eq 1. Rate constant for heterodimer formation (k_{obs}) is independent of initial concentrations of $P3_2$ and $\Delta289_2$. (C) Concentration independence of exchange rate constants (k_{obs}) and concentration dependence of initial rates indicate that the CheA dimers dissociate to free subunits prior to exchange. Dotted lines show the expected behavior for the lowest order associative mechanism where two dimers combine before exchange (see Appendix 1).

in Table 1 show the limits of $\Delta G^{\ddagger}_{d}$ and $\Delta S^{\ddagger}_{d}$ for the case of bond vibration and slower chain diffusion (5×10^8 s^{-1}). Taking the EP3 dissociation rate of 0.005 s^{-1} (25 °C) and a published value for the *E. coli* CheA dimer dissociation constant (0.2−0.4 μM) derived from the concentration dependence of CheA transphosphorylation (*13*), we obtain a bimolecular rate constant for association of the *E. coli* CheA subunits (k_r) that is on the order of 10^4 M^{-1} s^{-1} at 25 °C.

P3 Dissociation Is Coupled to Temperature and Chemical Induced Unfolding. The crystal structure of *T. maritima* CheA Δ289 indicates that each P3 subunit contributes to forming the hydrophobic core of the dimer. Thus, we investigated whether P3 unfolding was likely to coincide with subunit dissociation during exchange by comparing thermodynamic properties of P3 unfolding to those for the dissociation process (Table 1). Both TP3 and EP3 elute as dimers by GF and have a high helical content by circular dichroism (CD) spectroscopy that is consistent with the structure of P3 within the Δ289 dimer. Thermal unfolding of EP3 results in subunit dissociation and produces a flat featureless CD spectrum that indicates loss of helical content. Unfolding with temperature, as monitored by CD, fits a two-state mechanism for both EP3 and TP3 (Figure 5A). For EP3, the concentration dependence of the T_m establishes that unfolding is two-state and cooperative with dissociation; that is, folded subunits are dimeric and free subunits are unfolded (eq 5, Figure 5B). For EP3, thermal unfolding is at least 80% reversible at low concentrations and a linear relationship between $\ln(C_0)$ and T_m necessitates an unfolding process where the stoichiometry of product exceeds that of the reactant. Because the native form of EP3 is dimeric, the product of thermal unfolding must be a monomer (see Materials and Methods). ΔH_U for EP3 (63 kcal/mol at 59 °C, Table 1) obtained from van't Hoff analysis of the melting curve (eq 8) is relatively small compared to other four-helix bundles of similar size and structure (Table 2). EP3 unfolding with the chemical denaturant guanidine hydrochloride (GdnHCl) is reversible and gives $\Delta H_U = 36$ kcal mol^{-1} at 37 °C. After extrapolation to 59 °C with application of a constant ΔC_{pU} (see below), this value is in close agreement with that from thermal denaturation (GdnHCl unfolding extrapolated to 59 °C: $\Delta H_U = 60$ kcal mol^{-1}; $\Delta S_U = 155$ cal mol^{-1} K^{-1}; $\Delta G_U = 8.5$ kcal mol^{-1}; see Table 1).

TP3 unfolding monitored by CD occurs at much higher temperature ($T_m = 83-90$ °C, Figure 5A) than that of *E. coli* ($T_m = 59-68$ °C, Figure 5A) and is almost completely irreversible due to aggregation and precipitation of the unfolded product at temperatures beyond T_m. Differential scanning calorimetry (DSC) experiments confirm that aggregation accompanies thermal denaturation of TP3 (data not shown). In contrast, chemical unfolding of TP3 in GdnHCl is reversible; temperature dependence of ΔG_U so measured (Figure 6A) gave values of ΔH_U and ΔS_U for TP3 that are much higher than those of EP3 (Table 1). GF chromatography indicates that the unfolded state of TP3 in GdnHCl is

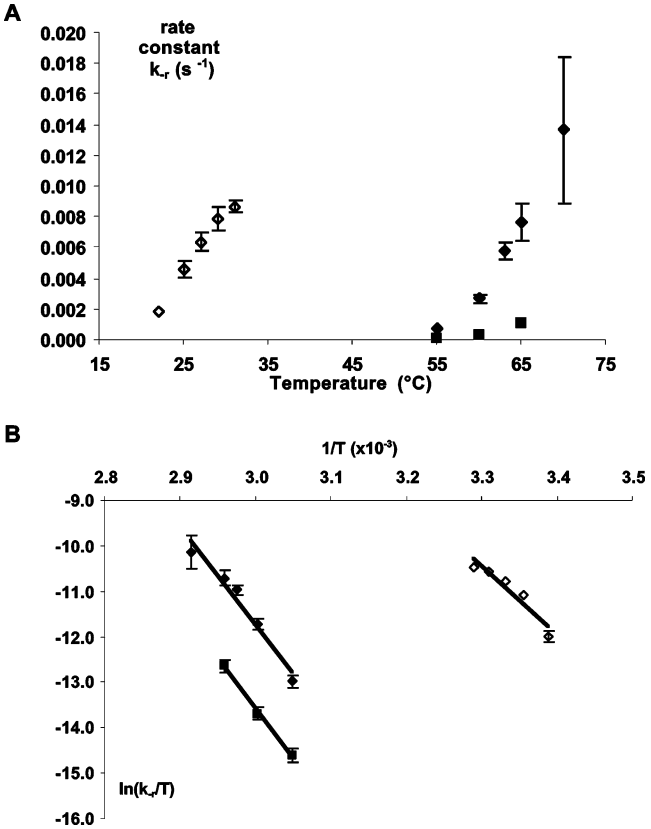

FIGURE 4: Temperature dependence of subunit dissociation rates. (A) Rate constants for dissociative subunit exchange for EP3 (◇), TP3 (◆), and TP3 with CheW (■) were measured by fitting the time course profile to eq 1. (B) Eyring plots for dimer dissociation of EP3 (◇), TP3 (◆), and TP3 in the presence of CheW (■) give the kinetic parameters shown in Table 1. Error bars are not shown for points where error is smaller than the point size.

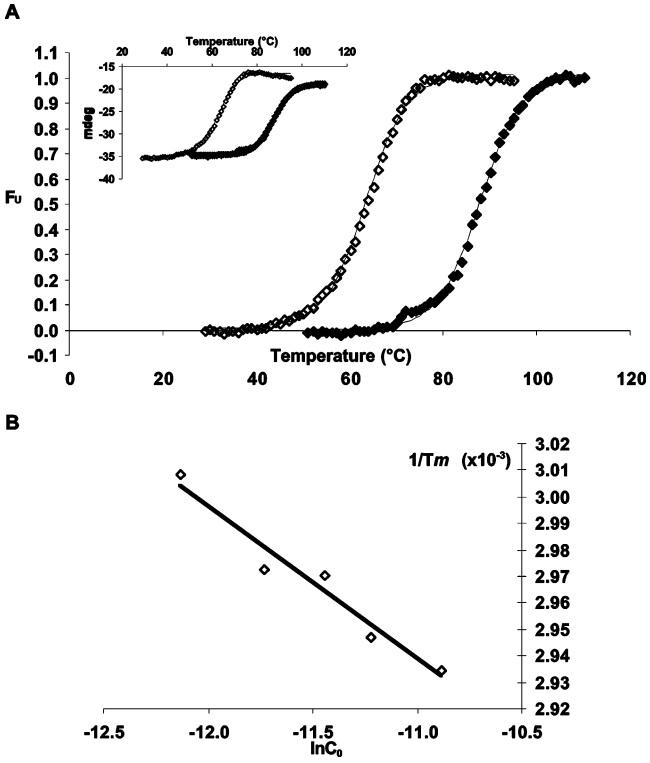

FIGURE 5: P3 dissociation accompanies temperature unfolding. (A) CD melting curves for EP3 (◇, 11 μM) and TP3 (◆, 16 μM). Ellipticity measured at wavelength 222 nm was converted to fraction unfolded (f_u) using the ellipticity values for the fully folded and fully unfolded state. TP3 (◆) melts at a much higher temperature (83−90 °C) than EP3 (◇) (59−68 °C). EP3 and TP3 have similar helical content by CD that agrees well with the P3 structure in Δ289. Inset shows raw CD signal (mdeg) after baseline correction. (B) Concentration dependence of T_m in EP3 thermal unfolding. Concentration dependence of the EP3 T_m fits a cooperative unfolding/dissociation model (eq 5). EP3 concentrations vary from 5 to 20 μM. Error bars are smaller than the point size.

monomeric (Figure 6B). Thermodynamic parameters from reversible GdnHCl unfolding agree well with parameters from thermal unfolding when adjusted to the T_m with the experimental or calculated ΔC_{pU} (GdnHCl unfolding extrapolated to 81 °C: ΔH_U = 178 kcal mol^{-1}; ΔS_U = 489 cal mol^{-1} K^{-1}; ΔG_U = 5 kcal mol^{-1}; see Table 1). This suggests that aggregation follows TP3 unfolding and is relatively slow.

Table 1: Thermodynamic and Kinetic Parameters for Unfolding and Dissociation in EP3 and TP3

	temp. (°C)	ΔH (kcal mol^{-1})	ΔS (cal mol^{-1} K^{-1})	ΔG (kcal mol^{-1})	ΔC_p (kcal mol^{-1} K^{-1})
		EP3			
ln K - (1/T)[a] (thermal unfolding)	59	63(±1)	168(±4)	7.6	NA
GdnHCl[b] (chemical unfolding)	37	36(±6)	80(±21)	10.7(±0.3)	1.0−1.2(1.0)
unfolding[c] extrapolated	27	24−26	41−48	11	NA
dissociation[d] activation (kinetics)	27	30(±6)	31−50	11−21	NA
		TP3			
ln K - (1/T)[a] (thermal unfolding)	81	172(±9)	466(±25)	7.2	NA
GdnHCl[b] (chemical unfolding)	40	125(±22)	329(±7)	21(±2)	1.0−1.2(1.5)
unfolding[c] extrapolated	63	148−152 (159)[e]	399−413 (435)[e]	13	NA
dissociation[d] activation (kinetics)	63	43 (±4)	57−76	13−23	NA

[a] ΔH_U and ΔS_U determined near T_m by van't Hoff relation (eq 8); $\Delta G_U = -RT \ln(C_0)$ since $K(T_m) = C_0$. [b] ΔG_U measured by chemical denaturation and application of the LEM (eq 9). ΔH_U, ΔS_U, and ΔC_{pU} taken from the temperature dependence of ΔG_U (eq 10). Experimental ΔC_{pU} values are given along with calculated values in parentheses. [c] Thermodynamic unfolding parameters extrapolated to the temperature where subunit exchange was measured with the experimental ΔC_{pU}. Ranges given for application of the minimum and maximum experimental ΔC_{pU} and calculated ΔC_{pU} (parentheses). [d] Activation parameters taken from Eyring plot of subunit dissociation (see Methods). Lower and upper limits of ranges reported for ΔG_d and ΔS_d derived from different preexponential factors reflecting either a bond vibration (Eyring, $A = k_B T/h$, $A = 6.2 \times 10^{12}$ s^{-1}) or chain diffusion (Kramer, $A = 5 \times 10^8$ s^{-1}) model. The range of values associated with choice of prefactor is much greater than the experimental error. For the case of slow chain diffusion, $\Delta H^{\ddagger}_d$ can be further corrected by subtracting an activation enthalpy associated with temperature dependence of water viscosity ($\Delta H^{\ddagger}_{(H_2O,vis)} = R\partial \ln \eta_o/\partial(1/T)$ = 3.8 kcal mol^{-1} (*48*, *43*), where η_o is the coefficient of viscosity for water. [e] Derived from calculated ΔC_{pU}.

Table 2: Thermodynamic and Structural Parameters for Coiled Coils[a]

	EP3	TP3	ROP	Apo-cyt b562	MCP (S461L)	GCN4
T_m (°C)[b]	60−70[b]	80−90[b]	71[b]	54	60[b]	70[b]
ΔH (kcal mol^{-1})	36 (37 °C)[c]	125 (40 °C)[c]	139 (71 °C)	47 (54 °C)	122 (60 °C)	63 (70 °C)
ΔH (kcal mol^{-1}) (extrapolated)[d]	0.67 (60 °C)	1.33 (60 °C)	1.55 (60 °C)	0.79 (60 °C)	0.27 (60 °C)	1.03 (60 °C)
ΔC_p(obsd) (kcal mol^{-1} K^{-1})	1.2	1.2	1.7	0.5	1.0	0.3
ΔC_p(calcd) (kcal mol^{-1} K^{-1})	1.0	1.5	1.4	0.5	2.6[e]	0.4
% hydrophobic ΔASA_U[f]	57	65	62	56	53	56
no. of helical residues	94	94	102	63	454	58
Protein Data Bank code	NA	1B3Q	1ROP	1APC	1QU7	2ZTA

[a] Thermodynamic parameters are given per dimer. References: ROP (*54*), apocyt b562 (*75*), MCP (*76*), GCN4 (*49*). [b] Concentration(s) at which T_m's for dimeric proteins were measured: 5−20 (EP3, TP3), 40 (ROP), 100 (MCP), and 500 μM (GCN4). [c] GdnHCl data (see Materials and Methods). [d] Extrapolated to 60 °C using ΔC_{pU}(obs) and given per helical residue for comparison. [e] ΔC_p(calcd) is overestimated because the MCPs are known to form structured free subunits (*56*, *57*). [f] Change in ASA on unfolding.

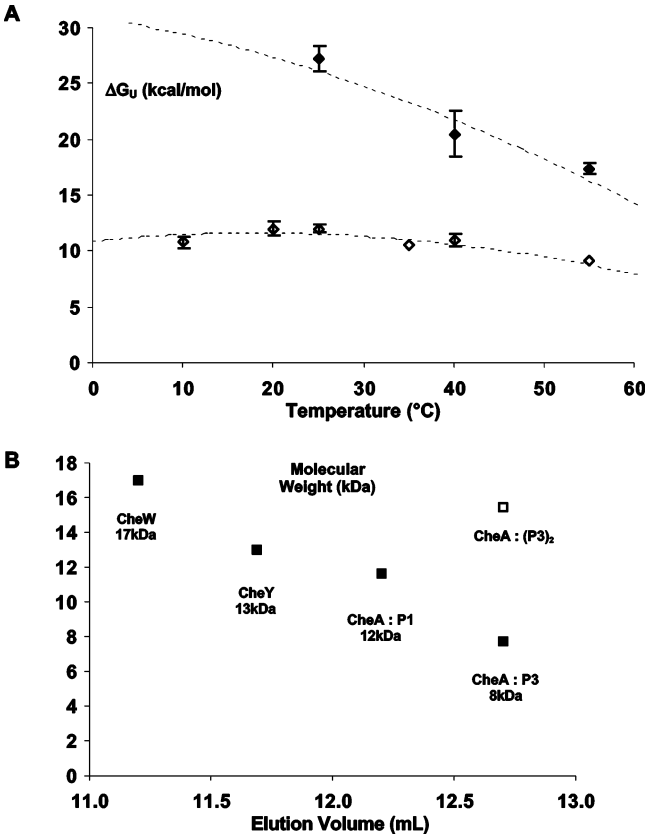

FIGURE 6: Chemical denaturation of TP3 and EP3. (A) ΔG_U for TP3 (◆) and EP3 (◇) as a function of temperature for GdnHCl-induced unfolding. For each temperature point, CD spectra at wavelength 222 nm were measured in increasing concentrations of GdnHCl and converted to ΔG_u. $\Delta G_u(H_2O)$ was determined by extrapolation to 0 M GdnHCl. ΔH_U, ΔS_U, and ΔC_{pU} extracted by fits to eq 10. Limits on the maximum value of ΔC_{pU} for TP3 were set by relating ΔH_U from chemical denaturation to that of thermal denaturation. (B) Unfolded TP3 is a monomer. TP3 and several other similar sized proteins were run in GF (Superose12) under 5M GdnHCl. The elution volume of unfolded TP3 corresponds to the molecular weight of a monomer. (□ indicates the predicted elution volume for a denatured P3 dimer).

CD spectra indicate similar unfolded states for EP3 and TP3 in 5 M GdnHCl and at high temperature. Both proteins in 5M GdnHCl have spectra that are flat and featureless, show little residual structure, and have molar ellipticities at 222 nm well within the range expected for unfolded coiled coils (EP3 $\theta_{222} = -3000$ °C cm^2 dmol^{-1}, TP3 $\theta_{222} = -5000$ deg cm^2 dmol^{-1}). Temperature denaturations converge to the same θ_{222} value for each protein and increasing temperature or GdnHCl concentration does not affect these values.

Heat Capacity Changes for P3 Unfolding and Subunit Exchange. If dissociation of the P3 domain couples to unfolding under conditions that destabilize the native state, unfolding may also accompany subunit exchange under physiological conditions. Comparison of thermodynamic parameters for unfolding with those for activation of subunit dissociation at the same temperature would provide insight into this issue. However, different temperatures are needed to monitor unfolding and subunit exchange, and thus knowledge of the change in heat capacity (ΔC_p) associated with at least one of these processes is needed to extrapolate its thermodynamic parameters to the temperature range where the other was measured.

Positive changes in ΔC_p are associated with protein unfolding and the exposure of hydrophobic groups to solvent (*24*, *29*). ΔC_p is a useful thermodynamic parameter for relating structural states because of its relative temperature independence and its correlation with polypeptide conformation. ΔC_p values can be predicted within a 10% accuracy for small globular proteins when structures of the native state are known (*24*, *29*). Specifically, the change in heat capacity with unfolding (ΔC_{pU}) is proportional to the changes in solvent accessible surface area (ΔASA) of nonpolar and polar groups exposed on unfolding (*24*, *29*). Predictions for coiled coils have greater error, as small changes in residue composition can drastically affect stability in these proteins (*16*, *30*, *31*). Nevertheless, statistical thermodynamic calculations (see Materials and Methods) for a set of four- and two-helix coiled coils provide estimates of ΔC_{pU} that agree well with experiment (Table 2). On the basis of the crystallographic structure of TP3 and a homology model of EP3 (Swiss-Model), we calculate a ΔC_{pU} of 1.5 kcal mol^{-1} K^{-1} for TP3 unfolding (16 cal mol^{-1} K^{-1} per residue) and a ΔC_p of 1.0 kcal mol^{-1} K^{-1} for EP3 unfolding (11 cal mol^{-1} K^{-1} per residue). These values are also consistent with the 9−15 cal mol^{-1} K^{-1} per residue range in ΔC_{pU} derived from measurements on small mesostable tetrameric coiled coils (*32*−*35*). The slightly higher TP3 ΔC_{pU} probably reflects the high hydrophobic contribution to its dimer interface (Table 2).

Experimental estimates of ΔC_{pU} for both TP3 and EP3 were difficult because both unfolded proteins aggregate at concentrations required for DSC. We instead relied upon the modest temperature dependence of ΔH_U apparent in GdnHCl unfolding and comparison between thermal and chemical denaturation to provide experimental support for the calculated ΔC_{pU} values. Fitting eq 10 to these data (Figure 6A)

gives ΔC_{pU} close to 1.0 kcal mol^{-1} for both EP3 and TP3, although there are significant errors in these values given the limited number of unfolding temperatures where complete series of GdnHCl melts were measured. Comparison of ΔH_U from GdnHCl denaturation with ΔH_U from thermal unfolding (which are derived at different temperatures) also gave ΔC_{pU} values for TP3 (1.2 kcal mol^{-1}) and EP3 (1.2 kcal mol^{-1}) that are consistent with the calculated and experimental values given above. Temperature and GdnHCl-induced unfolding of coiled coils give similar thermodynamic unfolding parameters, provided that both methods completely deplete helical content and the number of intersubunit salt bridges is low in the native state (*36*−*38*). TP3 and EP3 are predicted to have 2−4 salt bridges per 94 helical residues, much less than the 7 salt bridges per 56 helical residues in a designed leucine zipper where small differences between thermal ($\Delta G_U = 3$ kcal mol^{-1}) and GdnHCl unfolding ($\Delta G_U = 4$ kcal mol^{-1}) arise from charge screening by GdnHCl (*36*). Extrapolation of the GdnHCl unfolding parameters with either the calculated or experimental ΔC_{pU}'s reasonably predicts unfolding parameters of both EP3 and TP3 at their respective T_m's (Figure 5A and Figure 6A). Note that at T_m, $\Delta G_U = 7-8$ kcal mol^{-1} for a protein concentration of ~10 μM because subunit dissociation accompanies unfolding (eq 8).

ΔC_p for subunit dissociation ($\Delta C_p^{\ddagger}{}_d$) reflects the structural similarity between the transition state for dissociation (TS_d) and the unfolded state (U), provided that both are referenced to the native state, N. TP3 has a nearly linear Arrhenius plot (Figure 4B) that is best fit by $\Delta C_p^{\ddagger}{}_d$ of <0.4 kcal mol^{-1}. However, the errors and limited temperature range associate considerable uncertainty with this estimate. EP3 has a smaller temperature range over which the exchange kinetics can be measured, and thus not even a rough estimate of $\Delta C_p^{\ddagger}{}_d$ can be made reliably.

P3 Dissociation Activation Parameters More Closely Match Equilibrium Unfolding Parameters for EP3 than TP3. Similar thermodynamic parameters for P3 unfolding and subunit dissociation may imply corresponding conformational states in these two processes. However, comparison of thermodynamic parameters for unfolding with those of subunit dissociation must take into account temperature effects on enthalpy and entropy changes. Because ΔC_{pU} is necessarily positive for disrupting a hydrophobic core (≥1.0 kcal mol^{-1} for both EP3 and TP3), ΔH_U and ΔS_U are temperature-dependent. If substantial hydrophobic surface exposes in TS_d, then $\Delta H^{\ddagger}{}_d$ and $\Delta S^{\ddagger}{}_d$ could also be temperature dependent. Extrapolating ΔH_U and ΔS_U from the mid range of the GdnHCl denaturation experiments (40 °C) to the mid range of the exchange studies (63 °C) with application of either the experimental or calculated ΔC_{pU} gives values of ΔH_U (148−159 kcal mol^{-1}) and ΔS_U (399−435 cal mol K^{-1}) that are much greater than $\Delta H^{\ddagger}{}_d$ (39−43 kcal mol^{-1}) and $\Delta S^{\ddagger}{}_d$ (57−76 cal mol^{-1} K^{-1}) (Table 1). Thus, TS_d for TP3 subunit dissociation has different thermodynamic properties than U at the same temperature. Extrapolating ΔH_U and ΔS_U (measured at 37 °C) for EP3 with either the experimental or calculated ΔC_{pU} gives values of ΔH_U (24−26 kcal mol^{-1}) and ΔS_U (41−48 cal mol^{-1} K^{-1}) at 27 °C that are in reasonable agreement with $\Delta H^{\ddagger}{}_d$ (26−30 kcal mol^{-1}) and $\Delta S^{\ddagger}{}_d$ (31−50 cal mol^{-1} K^{-1}) (Table 1). Thus, unlike TP3, EP3 TS_d has thermodynamic properties similar to those of U. Although this analysis is based on estimates of ΔC_{pU}, the temperatures where chemical denaturation and exchange are measured do not differ greatly for either system. Thus, even if the ΔC_{pU} values were off by a factor of 3 (which would place them in an unreasonable range compared to similar systems), we would still conclude that the TP3 activation parameters for dissociation differ greatly from those for unfolding, whereas for EP3 they do not.

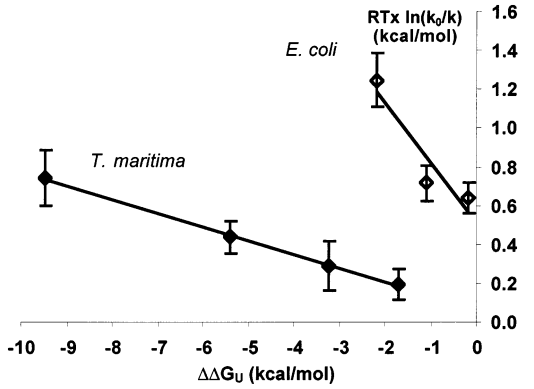

FIGURE 7: Changes in ΔG_u correlates more strongly with changes in $\Delta G_{d\ddagger}$ for EP3 than TP3. Subunit exchange rates and unfolding stability were altered by addition of glycerol, which destabilizes extended states relative to compact states. Plot of $\Delta\Delta G^{\ddagger}$ from rate constants and $\Delta\Delta G_U$ from thermal denaturation studies reflects how closely activation for subunit exchange relates to unfolding in EP3 and TP3. The larger slope (0.3) for EP3 compared to TP3 (0.07) signifies that the relationship between U and TS_d differs between EP3 and TP3.

Changes in the Rates of CheA Subunit Exchange Correlate More Strongly with Changes in Stability for EP3 than for TP3. Although comparison of unfolding parameters with those for subunit dissociation suggests that EP3 has a TS_d that thermodynamically resembles U, there may be less structural correspondence between the two states. Thus, to further investigate the conformation of TS_d for TP3 and EP3, we perturbed stability and exchange rates with glycerol, a cosolvent that disfavors extended conformations (*39*−*42*). Glycerol both slows exchange rates and stabilizes EP3 and TP3 by shifting respective T_m to higher temperatures. Even though TP3 thermal unfolding is irreversible, apparent T_m values should reflect relative stabilities because the TP3 melting curves are reversible up until the T_m and aggregation is likely slow compared to dissociation. Plotting the perturbation in unfolding free energy with glycerol ($\Delta\Delta G_U$, eq 11, Appendix 2) against $\Delta\Delta G^{\ddagger}{}_d$ (Figure 7), calculated from dissociation rates in the same glycerol concentrations (eq 12), gives a linear relationship for TP3 and an approximately linear relationship for EP3. Also, the slope (Φ) is larger for EP3 (0.3) than for TP3 (0.07). Thus, the relationship between U and TS_d differs in EP3 and TP3. Because glycerol destabilizes extended states, the closer correspondence between changes in $\Delta G^{\ddagger}{}_d$ and ΔG_U for EP3 compared to TP3 indicates a more extended (and likely unstructured) conformation for the TS_d of EP3 than for that of TP3.[3] However, since Φ ($\Delta\Delta G^{\ddagger}{}_d/\Delta\Delta G_U$) is much less than 1.0 for EP3, TS_d has less conformational similarity to the unfolded state than suggested by comparing the activation and unfolding parameters.

Receptor Coupling Protein CheW Inhibits CheA Subunit Dissociation. Addition of CheW to the $P3_2$ and $\Delta 289_2$

reactants slows the observed exchange reaction by a factor of 3−5 for *T. maritima* (Figure 4). CheW interacts strongly with $\Delta289_2$ and coelutes during size exclusion chromatography (estimated $K_D = 10^{-8}$ M by ITC). We found no interaction between *T. maritima* CheW and TP3 or domains TP3−TP4 by ITC (K_Ds > 1 mM not detected). Thus, inhibition of subunit exchange in our assay likely results from the direct interaction of CheW with $\Delta289_2$ through domain P5. If we model the kinetics of heterodimer formation by assuming that only k_{-r} for $\Delta289_2$ dissociation decreases with CheW binding, then k_{obs} reflects a decrease by a factor of 8 for k_{-r} of $\Delta289_2$.

DISCUSSION

Subunit exchange rates have been measured for the exchange reactions of two-helix coiled coils such as leucine zipper transcription factors (*30*, *46*) and tropomyosin (*47*); however, the mechanism by which stable four-helix coiled coils ($K_D < 1$ μM) exchange subunits under physiological conditions has not been extensively studied. Here we demonstrate that subunit exchange by the CheA dimer requires dissociation of the P3 dimerization domain and that the rate constant for P3 dissociation correlates with the stability of P3 versus unfolding. The exchange rate is highly temperature dependent and much slower for thermostable TP3 than for EP3 at a given temperature, despite high sequence similarity between the two proteins.

Thermal unfolding of EP3 unfolding is two-state, and loss of helical content is cooperative with subunit dissociation. GdnHCl unfolding of both EP3 and TP3 is also coupled to subunit dissociation. Cooperative unfolding/dissociation processes are common for other small dimeric proteins, such as the GCN4 leucine zipper (*30*, *48*, *49*), the P22 protein (*50*), streptococcal protein G (*51*), the Trp repressor (*22*), glutathione transferase A1-1 (*52*), and ROP (*53*, *54*). Our studies of CheA address an issue relevant to all of these systems: whether unfolding necessarily coincides with subunit dissociation when conditions favor the native state.

Thermodynamic parameters suggest that at least partial unfolding accompanies dissociation of EP3. The 9.1 kcal mol^{-1} free energy difference between the EP3 monomer and dimer (given by the reported K_D value of 0.2 μM, *13*) is similar to the predicted free energy for unfolding at the same temperatures (11 kcal mol^{-1}). Thus, the free EP3 subunits are close in energy to the unfolded state. Likewise, the thermodynamic activation parameters to form TS_d are similar to the equilibrium parameters for EP3 unfolding at the same temperature. The similar thermodynamic properties of EP3 TS_d and U could arise from these states having related conformations. However, in GCN4 coiled-coil unfolding, activation parameters also closely correspond to overall unfolding parameters, but a $\Delta C_p^{\ddagger}{}_U$ that is smaller than ΔC_{pU} indicates that the GCN4 coiled coil only partly unfolds in TS_U (*48*). Thus, when coiled coils transit from TS_U to U, a negative ΔH from exposing hydrophobic groups to solvent can offset a positive ΔH for breaking helix hydrogen bonds. Chain entropy and solvent entropy similarly compensate to produce only small thermodynamic differences between TS_U and U, even though TS_U is more compact. Thus, similar values for ΔH_U, ΔS_U, and $\Delta H_d^{\ddagger}$, $\Delta S_d^{\ddagger}$ of EP3 do not necessarily mean that TS_d and U are structurally similar.

To draw correspondence between the structure of TS_d and U, one could directly compare $\Delta C_p^{\ddagger}{}_d$ with ΔC_{pU}. However, the difficulty in obtaining accurate values of $\Delta C_p^{\ddagger}{}_d$ motivated us instead to investigate the relative effects of an agent known to disfavor extended states on P3 exchange rates and stabilities. Glycerol preferentially increases the chemical potential of water at the protein surface and thereby destabilizes extended conformations in which the protein ASA increases (*40*, *41*). Moreover, glycerol and other similar cosolvents lessen large amplitude conformational motions more prevalent when proteins unfold (*39*, *42*, *55*). The linear correlation between increasing EP3 dissociation activation energy and increasing stability with glycerol suggests that glycerol destabilizes TS_d relative to N within a significant fraction of how much it destabilizes U relative to N (0.3). Hence, EP3 TS_d has some extended structure, but not as much as indicated by the correlation between dissociation and equilibrium thermodynamic parameters (Table 1).

In contrast to EP3, thermodynamic parameters for TP3 unfolding differ considerably from those for activation of subunit dissociation. Extrapolating ΔH_U and ΔS_U to the temperature of the exchange studies (59 °C) gives values that are much greater than $\Delta H_d^{\ddagger}$ and $\Delta S_d^{\ddagger}$ (Table 1). Furthermore, changes in $\Delta\Delta G_d^{\ddagger}$ are only a small fraction of $\Delta\Delta G_U$ for TP3 (0.07) in the glycerol perturbation studies. Thus, the relationship of the high energy state in subunit dissociation to the unfolded state differs in TP3 and EP3. Differences between TP3 and EP3 in both TS_d and U could contribute to these discrepancies between the two proteins. However, the dissociation transition states likely distinguish the two systems because CD spectra for unfolded EP3 and TP3 indicate conformationally similar states. Furthermore, if the unfolded states were different, one would expect an unfolded state that was more, not less, energetically similar to TS_d for TP3 compared to EP3. The smaller activation parameters compared to unfolding parameters for TP3 and the glycerol perturbation studies then suggest that TP3 has a relatively compact TS_d that differs in energy and structure from U.

Subunit exchange rate constants for two-helix coiled coils vary greatly and correlate with dimer stability (leucine zippers ($10^{-2} - 10^{-3}$ s^{-1}) (*30*), Fos/Jun (0.2 s^{-1}) (*46*), tropomyosin (5×10^{-4} s^{-1}) (*47*)). In these systems, dissociation coincides with unfolding to disordered monomers, followed by concerted rapid folding and reassociation. This mechanism contrasts with the slow association ($k_r \sim 1$ M^{-1} s^{-1}) and very slow dissociation ($k_{-r} \sim 1 \times 10^{-7}$ s^{-1}) of the four-helix 280-residue cytoplasmic fragment of the *E. coli* Tsr chemoreceptor (*56*, *57*). Tsr receptor fragments also partially unfold during subunit dissociation, but their monomers have structure that must be dissolved for reassociation into dimer (*56*, *57*). Unlike Tsr, the TP3 monomer conformation does not prevent rapid reassociation into the dimer. Although the EP3 monomer and TS_d are close in energy to the unfolded state, the glycerol perturbation studies indicate

[3] Adding glycerol could also dampen molecular motions involved in crossing TS_d. Kramer's theory predicts that if glycerol does not affect $\Delta G_d^{\ddagger}$, relative time constants for dissociation ($k_{-r}{}^{-1}$) and relative viscosity (η_{rel}) should scale uniformly with increasing glycerol (*21*, *43*−*45*). Different slopes in the viscosity plots of EP3 and TP3 indicate that glycerol effects on stability dominate effects on increased solvent friction.

that the EP3 dimer does not have to completely unfold to dissociate. For TP3 and EP3 to retain compact structure as free monomers, they must sequester at least some of the hydrophobic surface exposed on subunit dissociation. This will limit nonspecific interactions and may explain why TP3 and EP3 will not exchange subunits with each other, despite conserving most of the residues in their respective dimer interfaces.

Considering the high similarity of TP3 and EP3 in helical structure and sequence (Figure 1D), the large differences in thermodynamic properties between these proteins is quite surprising (Table 2). A homology model of EP3 based on the TP3 structure predicts that TP3 exposes a greater percentage of hydrophobic surface area on unfolding, which could explain its enhanced thermal stability. However, EP3 should have a similar number of hydrogen bonds and expose comparable polar and nonpolar surface area on unfolding as another four-helix bundle of the same size: the ROP protein. In comparison to ROP, EP3 has a much smaller ΔH_U that may result from structural differences at the bundle ends (Table 2). ROP has an antiparallel arrangement of two helical hairpins in contrast to the EP3 parallel arrangement, lacks the N-terminal β-strands of EP3, and has shorter interhelical loops. TP3 has a similar ΔH_U as ROP and also contains a shorter interhelical linker that adds hydrophobic helix core capping residues absent in EP3. Thus, by nucleating folding of the helical hairpin in each subunit, the P3 interhelical loop could partly determine domain stability and mechanisms of association and folding. Changing the length and residue character of the ROP interhelical loop impacts stability, folding kinetics, oligomeric state, and topology (*31*, *58*−*62*). Of particular relevance to P3, systematic lengthening of the ROP interhelical loop correlates with a decrease in stability (*61*).

CheA subunit exchange (time constant of seconds to minutes) occurs on a slower time scale than the millisecond tuning of CheA activity by receptor occupancy but is commensurate with the time required for receptor adaptation (*63*, *64*). Both these fast and slow responses of chemotaxis depend on the receptor coupling protein CheW (*65*, *66*). CheW interacts strongly with CheA, localizes CheA and receptors to the poles of bacteria cells (*67*), and is necessary for the receptor clustering involved in signal amplification (*68*). The finding that CheW inhibits CheA subunit exchange by lowering the subunit dissociation rate by 8-fold indicates that complexes of CheA and CheW may stabilize the CheA dimer within the cell. Furthermore, inhibition of CheA dissociation by CheW provides insight into the mode of CheW interaction with CheA. CheW binds the P5 domain of CheA (*69*). P5 is homologous to CheW and conserves a hydrophobic surface at the end of two β-barrels that compose the common fold (*6*, *70*). This interface on CheW has been shown by NMR (*70*) and mutational studies (*71*, *72*) to interact with CheA; the analogous surface on P5 forms a symmetric interaction with itself in the crystal lattice of CheA Δ289 (*6*). Taken together, these data suggest that CheW may interact with CheA through a pseudosymmetric interface formed by residues conserved by both proteins (Figure 1A). However, the structure of CheA Δ289 places this interface remote from P3. Thus, our exchange data indicate that either CheW binding to P5 enhances interaction of P5 with P3 to stabilize P3 against conformational changes that lead to dissociation, or that CheW induces movement of the CheA domains to generate new stabilizing contacts within the dimer.

Varying degrees of P3 conformational destabilization accompany CheA subunit exchange in both *E. coli* and *T. maritima*. Unfolded subunits of EP3 and TP3 aggregate because structural specificity provided by the compact globular fold is lost. Aggregation of unstructured domains in thermophiles should be a severe problem as higher temperatures increase the strength of the hydrophobic effect. Given the large number of coiled-coil proteins present in cells and the similarities among their helical, hydrophobic association surfaces, mechanisms must limit nonspecific interactions between free subunits. For CheA, contacts with another protein (CheW) stabilize the dimer. Furthermore, the P3 monomers retain sufficient structure to prevent nonspecific interactions that lead to aggregation from the unfolded states. The degree of unfolding for EP3 and TP3 monomers correlates with the tendency of aggregation in the temperature range where exchange activates.

Thus, stable CheA dimers dissociate and redistribute subunits on a time scale of minutes. Although compact structure in these free subunits may be significantly destabilized, they retain specificity for native interactions and do not aggregate like their unfolded states. Recently, mutations within the interface regions of stable oligomers have been linked to the formation of disease causing aggregates (*73*, *74*). Our studies suggest that dimer destabilizing mutations may lead to aggregates by both increasing the concentration of free subunits and by destabilizing those subunits toward an unfolded state prone to nonspecific interactions.

ACKNOWLEDGMENT

We thank Bryan Beel, Melvin Simon, and Harold Scheraga for critical reading of this manuscript and Harry Gray for access to CD spectroscopy. C.M.Q. thanks the NIH for a predoctoral fellowship. We also thank the anonymous referees for their constructive criticism and helpful suggestions.

APPENDIX 1

Dissociative Dimer Exchange. Consider a reaction where two dimers (A_2 and B_2) dissociate into monomers (A and B) and then reassociate to form heterodimers (AB) with the kinetic scheme indicated in Figure 3A (left). If the dissociation and association rate constants of both reactants are the same (i.e., identical dimerization domains for A and B), then the rate equations for this process are

$$\frac{d[A_2]}{dt} = -k_{-r}[A_2] + k_r[A]^2$$

$$\frac{d[B_2]}{dt} = -k_{-r}[B_2] + k_r[B]^2$$

$$\frac{d[A]}{dt} = 2k_{-r}[A_2] - 2k_r[A]^2 - k_h[A][B] + k_{-h}[AB]$$

$$\frac{d[B]}{dt} = 2k_{-r}[B_2] - 2k_r[B]^2 - k_h[A][B] + k_{-h}[AB]$$

$$\frac{d[AB]}{dt} = k_h[A][B] - k_{-h}[AB]$$

If at time $t = 0$, $[A_2]_o = [B_2]_o$, then at any time t $[A_2] =$

$[B_2]$, $[A] = [B]$, and $[AB] = 2([A_2]_o - [A_2])$. If [A] and [B] are small, then the steady-state approximation applies and

$$\frac{d[A]}{dt} = \frac{d[B]}{dt} = 0$$

Solving for [AB] gives

$$[AB] = 2[A_2]_o\left(\frac{k_h k_{-r}}{k_h k_{-r} + 2k_{-h}k_r}\right)(1 - e^{-k_{obs}t})$$

$$k_{obs} = \frac{k_h k_{-r} + 2k_{-h}k_r}{k_h + 2k_r}$$

If $k_{-h} = k_{-r}$ and $k_h = 2k_r$ (because the collision frequency of A with B is twice that of A with A when $[A] = [B]$).

$$[AB] = [A_2]_o(1 - e^{-k_r t})$$

The rate of heterodimer formation depends only on the rate constant for homodimer dissociation (k_{-r}) and increases linearly with the concentrations homodimer reactants, provided they are initially equal. At long times $[AB] = [A_2]_o$ and $[A_2] = [B_2] = [A_2]_o/2$.

Associative Dimer Exchange. Consider a bimolecular reaction where two dimers (A_2 and B_2) associate, swap subunits, and then dissociate into heterodimers (AB) with the kinetic scheme indicated in Figure 3A (right). Assuming that heterodimers are kinetically and thermodynamically indistinguishable from homodimers leads to the following rate equations:

$$\frac{d[A_2]}{dt} = -k_1[A_2][B_2] + k_{-1}[AB]^2$$

$$\frac{d[B_2]}{dt} = -k_1[A_2][B_2] + k_{-1}[AB]^2$$

$$\frac{d[AB]}{dt} = 2k_1[A_2][B_2] - k_{-1}[AB]^2$$

If at time $t = 0$, $[A_2]_o = [B_2]_o$, then at any time t $[A_2] = [B_2]$ and $[A_2] = [A_2]_o - 1/2[AB]$.

For a statistical distribution of products at equilibrium, $2k_{-1} = k_1$. Then

$$\frac{d[AB]}{dt} = 2k_1[A_2]_o^2 - k_{-1}[A_2]_o[AB]$$

Solving for [AB] gives

$$[AB] = [A_2]_o(1 - e^{-2k_1[A_2]_o t})$$

Although this equation has a form similar to the one describing a dissociative mechanism, in the associative case the observed exponential rate constant depends on $[A_2]_o$.

For small t

$$e^{-2k_1[A_2]_o t} \cong 1 - 2k_1[A_2]_o t$$

and

$$[AB] = 2k_1[A_2]_o^2 t$$

Thus, at short times, initial rates are second order in reactant concentration and at long times $[AB] = [A_2]_o$ and $[A_2] = [B_2] = [A_2]_o/2$, as in the dissociative mechanism.

APPENDIX 2

In the presence of glycerol, we use the shift in melting temperature to approximate the change in the free energy of unfolding ($\Delta\Delta G_U$)

$$\Delta\Delta G_U = \Delta G_0(T_m) - \Delta G(T_m)$$

where $\Delta G_0(T_m)$ represents the change in Gibb's energy for unfolding in the absence of glycerol, $\Delta G(T_m)$ represents the change in Gibb's energy for unfolding in the presence of glycerol, and T_m is the melting temperature in the presence of glycerol.

From eq 6, $\Delta G_0(T_{m0}) = -RT_{m0} \ln C_0$, where T_{m0} = the melting temperature in the absence of glycerol.

If $-RT_{m0} \ln C_0 = X_0$, then $X_0 = \Delta H_0 - T_{m0}\Delta S_0$ and $\Delta S_0 = (\Delta H_0 - X_0)/T_{m0}$. Then $\Delta G_0(T_m) = \Delta H_0 - T_m(\Delta H_0 - X_0)/T_{m0}$ and $\Delta\Delta G_U = \Delta H_0 - T_m(\Delta H_0 - X_0)/T_{m0} - X$, where $X = -RT_m \ln C_0$.

On rearrangement,

$$\Delta\Delta G_U = \Delta H_0/T_{m0}(T_{m0} - T_m) + T_m/T_{m0}X_0 - X = \Delta H_0/T_{m0}(T_{m0} - T_m)$$

REFERENCES

1. Berg, H. C. (1975) *Nature 254*, 389−392.
2. Blair, D. F. (1995) *Annu. Rev. Microbiol. 49*, 489−522.
3. Falke, J. J., Bass, R. B., Butler, S. L., Chervitz, S. A. and Danielson, M. A. (1997) *Annu. Rev. Cell Dev. Biol. 13*, 457−512.
4. Wolanin, P. M., and Stock, J. B. (2003) in *Histidine Kinases in Signal Transduction* (Inouye, M. R. D., Ed.) pp 74−123, Academic Press, San Diego.
5. Swanson, R. V., Schuster, S. C., and Simon, M. I. (1993) *Biochemistry 32*, 7623−7629.
6. Bilwes, A. M., Alex, L. A., Crane, B. R., and Simon, M. I. (1999) *Cell 96*, 131−141.
7. Bilwes, A. M. P., S., Quezada, C. M., Simon, M. Crane B. R. (2003) in *Histidine Kinases in Signal Transduction* (Inouye, M. R. D., Ed.) pp 48−74, Academic Press, San Diego, CA.
8. Gegner, J. A., and Dahlquist, F. W. (1991) *Proc. Natl. Acad. Sci. U.S.A. 88*, 750−754.
9. Ellefson, D. D., Weber, U., and Wolfe, A. J. (1997) *J. Bacteriol. 179*, 825−830.
10. Kim, K. K., Yokota, H., and Kim, S. H. (1999) *Nature 400*, 787−792.
11. Falke, J. J., and Kim, S.-H. (2000) *Curr. Opin. Struct. Biol. 10*, 462−469.
12. Swanson, R. V., Bourret, R. B., and Simon, M. I. (1993) *Mol. Microbiol. 8*, 435−441.
13. Surette, M. G., Levit, M., Liu, Y., Lukat, G., Ninfa, E. G., Ninfa, A., and Stock, J. B. (1996) *J. Biol. Chem. 271*, 939−945.
14. Dyson, H. J., and Wright, P. E. (2002) *Curr. Opin. Struct. Biol. 12*, 54−60.
15. Dobson, C. M. (2003) *Nat. Rev. Drug Discov. 2*, 154−160.
16. Yu, Y. B. (2002) *Adv. Drug Deliv. Rev. 54*, 1113−1129.
17. Kweon, D. H., Chen, Y., Zhang, F., Poirier, M., Kim, C. S., Shin, Y. K. (2002) *Biochemistry 41*, 5449−5452.
18. Huber, R., T. A. Langworthy et al. (1986) *Arch. Microbiol. 144*, 324−333.
19. Gill, S. C., and von Hippel, P. H. (1989) *Anal. Bioch. 182*, 319−326.
20. Espenson, J. H. (1995) *Chemical Kinetics and Reaction Mechanisms*, McGraw-Hill, New York.
21. Bieri, O., and Kiefhaber, T. (2000) in *Frontiers in Molecular Biology*: *Mechanisms of Protein Folding*. (Pain, R. H., Ed.) pp 34−64, Oxford University Press, New York.

22. Gloss, L. M., and Matthews, C. R. (1998) *Biochemistry 37*, 16000−16010.
23. Marky, L. A., and Breslauer, K. J. (1987) *Biopolymers 26*, 1601−1620.
24. Makhatadze, G., and Privalov, P. L. (1995) *Adv. Prot. Chem. 47*, 307−420.
25. Lee, B., and Richards, F. M. (1971) *J. Mol. Biol. 55*, 379−400.
26. Creamer, T. P., Srinivasan, R., and Rose, G. D. (1995) *Biochemistry 34*, 16245−16250.
27. Creamer, T. P., Srinivasan, R., and Rose, G. D. (1997) *Biochemistry 36*, 2832−2835.
28. Peitsch, M. C. (1996) *Biochem Soc. Trans. 24*, 274−279.
29. Murphy, K. P., and Freire, E. (1992) *Adv. Prot. Chem. 43*, 313−361.
30. Wendt, H., Berger, C., Baici, A., Thomas, R. M., and Bosshard, H. R. (1995) *Biochemistry 34*, 4097−4107.
31. Peters, K., Hinz, H. J., and Cesareni, G. (1997) *Biol. Chem. 378*, 1141−1152.
32. Betz, S. F., and DeGrado, W. F. (1996) *Biochemistry 35*, 6955−6962.
33. Fairman R., C., H. G., Mueller, L., Lavoie, T. B., Shen, L., Novotny, J., and Matsueda, G. R. (1995) *Protein Sci. 4*, 1457−1459.
34. Hagihara, Y., Oobatake, M., and Goto, Y. (1994) *Protein Sci. 3*, 1418−1429.
35. Wilcox W., and Eisenberg, D. (1992) *Protein Sci. 1*, 641−653.
36. Phelan, P., Gorfe, A. A., Jelesarov, I., Marti, D. N., Warwicker, J., and Bosshard, H. R. (2002) *Biochemistry 41*, 2998−3008.
37. Guo, Y., Kammerer, R. A., and Engel, J. (2000) *Biophys. Chem. 85*, 179−186.
38. Boice, J. A., Dieckmann, G. R., DeGrado, W. F., and Fairman, R. (1996) *Biochemistry 35*, 14480−14484.
39. Butler, S. L., and Falke, J. J. (1996) *Biochemistry 35*, 10595−10600.
40. Durr, E., and Jelsarov, I. (2000) *Biochemistry 39*, 4472−4482.
41. Timasheff, S. N. (1993) *Annu. Rev. Biophys. Biomol. Struct. 22*, 67−97.
42. Liu, Y., and Bolen, D. W. (1995) *Bochemistry 34*, 12884−12891.
43. Perl, D., Jacob, M., Bano, M., Stupak, M., Antalik, M., and Schmid, F. X. (2002) *Biophys. Chem. 96*, 173−190.
44. Bhattacharyya, R. P., and Sosnick, T. R. (1999) *Biochemistry 38*, 2601−2609.
45. Jacob, M., and Geeves, M., and Holtermann, G., and Schmid, F. X. (1999) *Nat. Struct. Biol. 6*, 923−926.
46. Patel, L. R., Curran, T., and Kerppola, T. K. (1994) *Proc. Natl. Acad. Sci. U.S.A. 91*, 7360−7364.
47. Ozeki, S., Kato, T., Holtzer, M. E., and Holtzer, A. (1991) *Biopolymers 31*, 957−966.
48. Ibarra-Molero, B., Makhatadze, G. I., and Matthews, C. R. (2001) *Biochemistry 40*, 719−731.
49. Thompson, K. S., Vinson, C. R., and Freire, E. (1993) *Biochemistry 32*, 5491−5496.
50. Milla, M. E., and Sauer, R. T. (1994) *Biochemistry 33*, 1125−1133.
51. Alexander, P., Orban, J., and Bryan, P. (1992) *Biochemistry 31*, 7243−7248.
52. Wallace, L. A., Sluis-Cremer, N., and Dirr, H. W. (1998) *Biochemistry 37*, 5320−5328.
53. Lassalle, M. W., and Hinz, H.-J. (1998) *Biochemistry 37*, 8465−8472.
54. Steif, C., Weber, P., and Hinz, H.-J. (1993) *Biochemistry 32*, 3867−3876.
55. Wang, A., Robertson, A. D. and Bolen, D. W. (1995) *Biochemistry 34*, 15096−15104.
56. Seeley, S. K., Wittrock, G., Thompson, L. K., and Weis, R. M. (1996) *Biochemistry 35*, 16336−16345.
57. Murphy, O. J. I., Yi, X., Weis, R. M., and Thompson, L. K. (2001) *J. Biol. Chem. 276*, 43262−43269.
58. Nagi, A. D., Anderson, K. S., and Regan, L. (1999) *J. Mol. Biol. 286*, 257−265.
59. Lassalle, M. W., Hinz, H. J., Wenzel, H., Vlassi, M., Kokkinidis, M., and Cesareni, G. (1998) *J. Mol. Biol. 279*, 987−1000.
60. Lassalle, M. W., and Hinz, H. J. (1998) *Biochemistry 37*, 8465−8472.
61. Nagi, A. D., and Regan, L. (1997) *Folding & Des. 2*, 67−75.
62. Munson, M., Anderson, K. S., and Regan, L. (1997) *Folding & Des. 2*, 77−87.
63. Segall, J., Manson, M. D., Berg, H. C. (1982) *Nature 296*, 855−857.
64. Springer, M. S., Goy, M. F., and Adler, J. (1979) *Nature 280*, 279−284.
65. Parkinson, J. S., and Kofoid, E. C. (1992) *Annu. Rev. Genet. 26*, 71−112.
66. Alex, L. A., and Simon, M. I. (1994) *Trends Genet. 10*, 133−138.
67. Maddock, J. R., and Shapiro, L. (1993) *Science 259*, 1717−1723.
68. Gestwicki, J. E., and Kiessling, L. L. (2002) *Nature 415*, 81−84.
69. Bourret, R. B., Davagnino, J., and Simon, M. I. (1993) *J. Bacteriol. 175*, 2097−2101.
70. Griswold, I. J., Zhou, H., Matison, M., Swanson, R. V., McIntosh, L. P., Simon, M. I., and Dahlquist, F. W. (2002) *Nat. Struct. Biol. 9*, 121−125.
71. Boukhvalova, M., VanBruggen, R., and Stewart, R. C. (2002) *J. Biol. Chem. 277*, 23596−23603.
72. Boukhvalova, M., Dahlquist, F. W., and Stewart, R. C. (2002) *J. Biol. Chem. 277*, 22251−22259.
73. Cardoso, R. M. F., Thayer, M. M., DiDonato, M., Lo, T. P., Bruns, C. K., Getzoff, E. D, and Tainer, J. A. (2002) *J. Mol. Biol. 324*, 247−256.
74. Rakhit, R., Cunningham, P., Furtos-Matei, A., Dahan, S., Qi, X. F., Crow, J. P., Cashman, N. M., Kondjewski, L. H., and Chakrabartty, A. (2002) *J. Biol. Chem. 277*, 47551−47556.
75. Robinson, C. R., Liu, Y., O'Brien, R., Sligar, S. G., and Sturtevant, M. (1998) *Protein Sci. 7*, 961−965.
76. Wu, J., Long, D. G., and Weis, R. M. (1995) *Biochemistry 34*, 3056−3065.

BI0352419